Altered patterning of interneuron progenitors in Down syndrome

Yathinder Giffin-Rao, Bennett Strand, Margaret Medo, Aratrika Keshan, Roger A. Daley. Jr., Sruti Mohan, Samuel Dantienne, Bradley Levesque, Lindsey Amundson, Leslie Huang, Rebecca Reese, Daifeng Wang[3], Su-Chun Zhang[2], Anita Bhattacharyya[1]

Waisman Center, University of Wisconsin-Madison, Madison WI 53705
[1]Department of Cell and Regenerative Biology, School of Medicine and Public Health, University of Wisconsin-Madison, Madison WI 53705
[2]Departments of Neuroscience and Neurology, School of Medicine and Public Health, University of Wisconsin-Madison, Madison WI 53705
[3]Department of Biostatistics and Medical Informatics, University of Wisconsin-Madison, 1500 Highland Avenue, Madison WI 53705

Correspondence:
Anita Bhattacharyya: Waisman Center and Department of Cell and Regenerative Biology, University of Wisconsin-Madison School of Medicine and Public Health, Madison, WI 53705, USA; Phone: (608) 265-6142; E-mail: bhattacharyy@waisman.wisc.edu.

Acknowledgements
We thank members of the Zhang lab, particularly Yunlong Tao, for helpful comments and members of the Bhattacharyya lab, Jose Martinez and Anna Baker, for technical assistance. We also thank Karla Knobel, Emily Fares, MBF technical support, Manuel Casanova and Ken Fish for guidance on stereology. We thank S. Splinter-BonDurant, D. Pavelec, and M.E. Berres at the UW-Madison Biotechnology Center for technical assistance. This work was supported by NIH grants R03HD083538 and R21NS105339, and funding from UW-Madison and the Wisconsin Alumni Research Foundation to A.B. This study was supported in part by a core grant to the Waisman Center from the National Institute of Child Health and Human Development (U54 HD090256).

ABSTRACT
Multiple developmental processes go awry in Down syndrome (DS, trisomy 21, Ts21), the most common genetic cause of intellectual disability and a complex multigene disorder. DS individuals have smaller brains with reduced volume of frontal and temporal lobes, including hippocampus. This smaller brain volume corresponds to fewer neurons in the DS cortex measured at pre- and post-natal stages, implicating impaired neurogenesis during development. We employ Ts21 human induced pluripotent stem cells (iPSCs) and *isogenic* controls to identify disrupted interneuron developmental processes in DS. Interneuron progenitor specification, proliferation and migration is largely controlled by integrating known morphogen gradients, sonic hedgehog (SHH) and Wingless (WNT), and we find that Ts21 progenitors have altered patterning and generate different progenitor populations. Specifically, we find expression of WNT signaling genes is reduced and expression of GLI genes that regulate WNT and SHH signaling in this population is increased in Ts21 interneuron progenitors, suggesting Ts21 progenitors are patterned more ventrally and less caudally. Altered patterning affects lineage decisions and, in fact, fewer caudal interneuron progenitors expressing the transcription factor COUP-TFII differentiate from Ts21 iPSCs. In mouse, COUP-TFII+ progenitors are found in more caudal regions of the neurogenic regions, thus linking the patterning changes to altered generation of interneuron subpopulations. These data identify affected progenitor subpopulations in Ts21 and suggest that abnormal patterning of human Ts21 interneuron progenitors alters the generation of interneurons in DS and contributes to the reduced neurogenesis in DS.

INTRODUCTION
To achieve complex functioning, the human cortex has evolved larger superficial layers and greater reliance on interneurons than other mammals. Cortical interneurons are much more numerous and much more complex than in mice in order to enable the complex functions unique to humans. Many human neuropsychiatric disorders and disorders characterized by intellectual disability are linked to defects in cortical interneuron development and function. Maldevelopment of interneurons can lead to abnormal numbers, subtypes and/or placement of neurons that significantly affect the functioning of the cortex, leading to cognitive impairment. The most common of these is Down syndrome (DS, trisomy 21, Ts21), a complex multigene disorder caused by trisomy 21.

Based on decades of research on mouse embryos, the development of interneurons is exquisitely dependent on morphogen cues. Interneuron progenitors are specified and proliferate in the three neurogenic areas of the ventral telencephalon: the lateral, medial, and caudal ganglionic eminences (LGE, MGE and CGE). Dorsal-ventral patterning is dependent on a Sonic hedgehog (SHH) signaling gradient for ventralization of the neural tube (Gulacsi and Anderson, 2006; Li et al., 2009; Xu et al., 2005). SHH signaling is balanced by dorsalizing signals, primarily via WNT signaling (Li et al., 2009). A gradient of WNT signaling is also primarily responsible for rostrocaudal patterning. Thus, the integration of SHH and WNT signaling is necessary for proper spatial specification of interneuron progenitors. Specific spatially-defined subpopulations of progenitors with distinct transcriptional profiles each ultimately give rise to specific interneuron subtypes, thus creating the diversity of interneurons in the cortex. The MGE is the primary source of interneurons in mice giving rise to 70% of the total cortical interneurons including parvalbumin (PV)+, calbindin (CB)+ and somatostatin (SST)+ subtypes. MGE progenitors express the transcription factor NKX2.1 whose expression is regulated by SHH (Du et al., 2008; Xu et al., 2010; Xu et al., 2008). While the mechanisms involved in the generation of MGE cells are well studied, much less is known about the development of other regions. CGE progenitors express the transcription factor COUP-TFII that is also expressed by progenitors in the caudal MGE. The CGE gives rise to vasoactive intestinal polypeptide (VIP)+, calretinin (CR)+, reelin+ and neuropeptide Y (NPY)+ interneurons in mouse.

The brains of DS individuals are smaller (Becker et al., 1991; Davidoff, 1928; Schmidt-Sidor et al., 1990; Wisniewski, 1990); brain volume is reduced in frontal and temporal areas of the cortex, including the hippocampus (Emerson et al., 1995; Kesslak et al., 1994; Wisniewski, 1990). Subcortical areas, in contrast, do not appear to be smaller in DS. Morphological analysis of pre and postnatal DS brains over the past 90 years has consistently revealed that there are fewer neurons in the developing and mature DS brain (Becker et al., 1991; Benda, 1947; Colon, 1972; Davidoff, 1928; Golden and Hyman, 1994; Ross et al., 1984; Takashima et al., 1981; Wisniewski et al., 1984), underlying the reduced volume and implicated reduced neurogenesis as a feature in DS (Lott and Dierssen, 2010). More recent work suggests that maldevelopment of the cortex in DS includes both altered neurogenesis early in development and altered gliogenesis and myelination later in development (Olmos-Serrano et al., 2016). Thus, multiple developmental processes are affected in DS.

Ross et al., describe the presence of fewer granular cells in upper layers throughout the cortex and suggest that fewer aspinous stellate interneurons are present (Ross et al., 1984). Our own *in vitro* data on DS fetal tissue corroborates that neuron reductions include GABAergic neurons (Bhattacharyya et al., 2009). We and others have modeled interneuron development using trisomy 21 iPSCs and our research group found that Ts21 iPSCs generate fewer CR+ neurons, both *in vitro* and *in vivo* (Huo et al., 2018)**.** These results align with human fetal cortical neuropathology and confirm that we can model developmental deficits interneurons using Ts21 iPSCs. Yet, recent data seems to contradict these *in vivo* and *in vitro* findings (Xu et al., 2019). We sought to address this controversy by carefully studying interneurons and interneuron progenitor subtypes in Down syndrome using post-mortem brain tissue and isogenic control and trisomy 21 iPSCs. We show that some interneuron populations are altered, while others are not. This information helps us better understand basic mechanisms of human interneuron development and reveals how mistakes can lead to intellectual disability.

RESULTS

Fewer neurons in DS cortex

Histopathological observations, though limited, reveal accumulation of fewer neurons, primarily in superficial layers of the cortex in DS (Golden and Hyman, 1994; Ross et al., 1984; Weitzdoerfer et al., 2001). Based on morphology, the data suggest that the neuron reductions include fewer aspinous stellate interneurons (Ross et al., 1984). We sought to determine whether there is a reduction in interneurons, and if so, to define which interneuron subtypes are altered, using immunohistochemical markers in post-mortem DS cortex. We analyzed post-mortem superior temporal gyrus (STG) from four DS and four age-matched control male individuals (ages 15-35) (**Figure 1A)**. These young adult ages are similar to those used in the previous morphological assessment that revealed fewer interneurons in DS (Ross et al., 1984) and were chosen to avoid the early onset degeneration that that has been shown to occur in DS as early as age 35. In addition, we analyzed the STG for several reasons: 1) thin STG is a consistent gross abnormality in DS brain (Becker, 1991; Mito et al., 1991); 2) alterations in neuron density and lamination in the STG occur during DS cortical development (Golden and Hyman, 1994); and 3) the STG is an association cortex and is likely to be involved in the characteristic intellectual impairment in DS. Immunocytochemistry and design-based stereology were used to quantify neuronal populations in sections (Perl et al., 2000; West, 2013) to ensure unbiased, efficient, and more reliable results than other ad hoc quantitative analyses (Boyce et al., 2010). Importantly, the method takes into account the gross size differences of DS brains. We used the Optical Fractionator Probe method (Stereo Investigator, MBF) to uniformly sample and estimate cell number together with the Cavalieri probe method to estimate volume (West et al., 1991). Our results show a reduced density of NeuN+ cells, corroborating the reduction in the number of neurons in DS cortex (**Figure 1B**; Control = $8.33 \times 10^6 \pm 0.79 \times 10^6$, DS= $0.49 \times 10^6 \pm 0.15 \times 10^6$, p=0.029, N=4). Using parvalbumin (PV) to identify the predominant interneuron subtype, we observed no difference in this population density between DS and controls (Control = $0.98 \times 10^6 \pm 0.18 \times 10^6$, DS= $0.89 \times 10^6 \pm 0.24 \times 10^6$, p=0.89, N=4). However, using calretinin (CR) as a marker of upper layer interneurons, our results show that the density of CR+ cells may be reduced in adult DS STG (Control = $1.74 \times 10^6 \pm 0.14 \times 10^6$, DS= $1.19 \times 10^6 \pm 0.23 \times 10^6$, p=0.11, N=4).

Ventralization of Ts21 iPSC results in altered patterning

Our *in vivo* results corroborate historical data and suggest that neurogenesis is affected in DS. Recent work from our research group and others using hPSCs *in vitro* has shown that the generation of interneuron subtypes is differentially altered by Ts21 (Huo et al., 2018; Xu et al., 2019). The results indicate that SST+ and CR+ interneurons are altered, although the results are discordant. To understand the foundational steps that lead to interneuron generation, we focused on development of interneuron progenitors to gain insight into early developmental events that go awry in DS cortical development. We initially analyzed one pair of newly established human Ts21 isogenic iPSCs to distinguish phenotypes due to trisomy 21 from variation between individuals and cell lines. To generate cortical interneuron progenitors, we ventralized neural progenitor cells with exogenous addition of SHH, indicated by the expression of the transcription factor NKX2.1 (**Figure 2A**) (Liu et al., 2013). Immunofluorescence of progenitors at Day 17, when cells initially acquire their positional phenotype (e.g. rostral vs. caudal and dorsal vs. ventral), indicates that both control and Ts21 progenitors respond to SHH

by expressing NKX2.1, as expected (**Figure 2B**). A population of COUP-TFII+ progenitors is also generated through ventralization with SHH (**Figure 2B**).

Based on mouse studies, NKX2.1+ and COUP-TFII+ populations are not mutually exclusive. While NKX2.1 is expressed in MGE, COUP-TFII is expressed in two spatial subpopulations of cortical interneuron progenitors: CGE and caudal MGE (Anderson, 2002; Anderson et al., 2002; Campbell, 2003; Parnavelas et al., 2000; Wilson and Rubenstein, 2000). These two COUP-TFII+ populations can be distinguished by NKX2.1 expression (Alfano et al., 2014; Kanatani et al., 2008; Lodato et al., 2011; Reinchisi et al., 2012); MGE progenitors express only NKX2.1, CGE progenitors express only COUP-TFII, while caudal MGE progenitors express both. To investigate whether there are differences in these subpopulations in Ts21 ventralized progenitors compared to controls, we looked more carefully at the specification of these cells. The percentage of MGE progenitors, as defined by NKX2.1+ COUP-TFII- expression, is higher in Ts21 ventralized progenitors in our isogenic pair (Control = 11.97 ±3.07, Ts21= 38.25 ± 7.53, p=0.0043) (**Figure 2C**). A similar pattern of increased MGE progenitors in Ts21 was validated in three additional distinct control and Ts21 iPSC lines (Control = 14.21 ± 1.822, Ts21= 21.15 ± 6.91, p=0.3964) **(Figure 2C)**. A subpopulation of the NKX2.1+ cells also express COUP-TFII when differentiated from both control and Ts21 cells, suggesting that ventralization solely by SHH in this human paradigm results in a caudal fate for some NKX2.1+ cells (**Figure 2D**). These cells represent caudal MGE-like cells and quantification indicates that fewer NKX2.1+COUP-TFII+ cells differentiate from Ts21 iPSCs compared to isogenic controls (Control = 32.66 ± 10.57, Ts21= 18.37 ± 6.81, p=0.0402). This pattern of decreased caudal MGE cells was validated in three distinct non-isogenic control and Ts21 iPSC lines (Control = 16.15 ± 3.01, Ts21= 6.72 ± 3.23, p=0.1914) (**Figure 2D**). Similarly, quantification of COUP-TFII+, NKX2.1- cells that represent CGE-like progenitors revealed fewer of these cells generated from Ts21 iPSCs compared to isogenic controls (Control = 12.83 ± 1.31, Ts21= 5.42 ± 1.30, p=0.0034)(**Figure 2E**), a result validated in three distinct non-isogenic control and Ts21 iPSC lines (Control = 13.18 ± 1.00, Ts21= 4.46 ± 1.55 p=0.300) (**Figure 2E**). It is important to note that while the percentage of MGE and caudal MGE subpopulations varied in progenitors differentiated from different iPSCs , both the proportion and pattern of CGE progenitors was preserved in all iPSC lines. We next asked whether these differences in Ts21 iPSC-derived progenitors recapitulate *in vivo* development by mining published microarray data from human fetal DS brain and found decreased expression of COUP-TFII, but not NKX2.1 in human fetal DS brain i*n vivo* (Olmos-Serrano et al., 2016) (**Figure 2F**).

Taken together, the results indicate that ventralization of Ts21 iPSCs results in altered patterning, specifically reduced caudal/posterior patterning, as indicated by the decreased expression of COUP-TFII and fewer COUP-TFII+ cells in the NKX2.1+ population. Ts21 progenitors show an increase in the proportion of NKX2.1+ COUP-TFII- MGE cells concomitant with a decrease in the proportion of COUP-TFII+ CGE cells. These results suggest that Ts21 leads to decreased generation of an important source of progenitors (CGE) for calretinin interneurons, thus providing a correlation between decreased calretinin neurons in DS cortex with decreased CGE progenitors in Ts21 iPSCs.

Altered SHH/WNT signaling in Ts21 ventralized progenitors revealed by transcriptomics.

In addition to providing rigorous phenotypic data, isogenic pairs of Ts21 and control iPSCs are extremely valuable for molecular profiling where variation between individuals and cell lines can be amplified and mask subtle differences. Unbiased transcriptional analysis (microarray) of Day 25 ventralized progenitors from two distinct sets of isogenic control and Ts21 iPSCs (WC24 clones B and M; DS2U and DS1) shows that there are differences in the number of genes whose expression is changed in Ts21 versus controls (**Figure 3A**). The two sets of cells have distinct and overlapping differentially expressed genes (**Figure 3B**) using fold change of 1.3. Genes on human chromosome 21 are generally increased in expression as expected for Ts21, but the number of genes that are over-expressed is different between the two isogenic pairs (**Figure 3C**). To define the biological processes that define the differences in Ts21 progenitors, we performed two analyses. First, we tested the entire target set from each pair of cells for enrichment of different GO processes. This analysis identified a number of common general processes that were up regulated or down regulated (**Figure 3 D, E**) across the two pairs including pathways that are generally involved in nervous system development. Shared down-regulated pathways include nervous system development and neural progenitor proliferation. Second, we overlaid differentially expressed genes identified from each isogenic pair on a functional interaction network and identified

gene clusters that were affected (**Figure 3F**). This analysis identified more common pathways between the two pairs including both dorso-ventral and anterior-posterior patterning, cell proliferation and WNT signaling (**Table 1**). In summary, enrichment analysis of the differentially expressed genes in two isogenic pairs of Ts21 and control progenitors reveals molecular mechanisms for altered patterning observed in Ts21 progenitors. WNT signaling emerges as a critical affected pathway in Ts21 progenitors.

Quantitative PCR for specific genes in the WNT pathway validated that expression of WNT pathway genes was reduced in Ts21 progenitors **(Figure 3 G, H, I**). Expression of SHH effector genes was also reduced and the expression of GLI genes that provide crosstalk between SHH and WNT pathways was altered **(Figure 3 G, H, I)**. Decreased expression of AXIN2 and increased expression of GLI3 corroborates expression in human fetal DS brain *in vivo* [15] **(Figure 3 G, H, I)**. These data indicate that Ts21 interneuron progenitors have altered response to WNT and SHH, raising the hypothesis that altered signaling results in mis-specification and/or proliferation that ultimately leads to decreased numbers of interneurons.

Single cell RNA-Seq reveals differences in subpopulations in Ts21

The results thus far suggest that there is a shift in the production of ventral neural progenitor cell subpopulations in Ts21 in response to SHH. To identify different progenitor subpopulations and define gene expression differences in the different subpopulations, we carried out single cell RNA sequencing (scRNA-Seq) experiments using one pair of isogenic Ts21 and control iPSC-derived progenitors (WC24) at Day 17 that had been ventralized with SHH. The initial principal component analysis (PCA) comparing Ts21 to controls produced a t-SNE plot showing almost complete segregation of the control and Ts21 neural progenitor cells (**Figure 4A**). The most highly expressed genes that drive this difference were associated with the cell cycle**.** SHH acts as a mitogen as well as a morphogen and so altered response to SHH could manifest in proliferation. We thus queried the cell cycle of the progenitors using Seurat (Butler et al., 2018) to score cells based what known cell cycle gene markers they express. This analysis enables the quantification of cells in each cell cycle phase. The results show that the number of cells in each cell cycle phase, as assessed by expression of PCNA, TOP2A, MCM6 and MKI67, is similar in Ts21 and control progenitors (**Figure 4B**).

We next asked if these two subpopulations of cells had differences in proliferation, as suggested by the initial PCA analysis. We directly quantified cell cycle kinetics in Ts21 and control progenitor subpopulations (one isogenic pair, WC24) by pulsing cells with EdU for 12 hours to label dividing cells and co-labeling with either NKX2.1 or COUPTF-II to determine the number of cells that were both EdU+ and positive for each transcription factor. The results show that there is a small but statistically significant increase in the percentage of NKX2.1+/EdU+ in the Ts21 cells compared to their isogenic controls (**Figure 4C**). Yet, this difference was not validated in an additional three Ts21 and control iPSC lines, indicating that there is no consistent difference in the proportion of NKX2.1+ cells that are dividing in Ts21 and highlighting the need to validate results from one set of iPSCs with others. In contrast, there are fewer proliferating COUP-TF-II+ cells in Ts21 progenitors (**Figure 4D**). Taken together, these results show that Ts21 ventralized subpopulations have different cell proliferation properties and that there are fewer COUP-TFII+ cell that are dividing in Ts21 while there is no difference in the NKX2.1+ subpopulation. These results further indicate that not all progenitor populations are equally affected in Ts21.

To determine what subpopulation of neural progenitor cells were present in the culture and the effect of Ts21 on these sub-populations, we used the Seurat R analysis program to regress out all the cell cycle genes so that the underlying gene markers could be used by the PCA analysis to segregate the populations (Butler et al., 2018) (**Figure 5A**). In order to determine how Ts21 was affecting the sub-population of cells, we next used canonical correspondence analysis (CCA) to segregate the population of cells (Zhang et al., 2019). Unlike PCA analysis, CCA analysis focuses on those genes that cells share in common rather than segregating them on highly differentially expressed genes. The resulting CCA t-SNE plot shows the euploid and TS21 NPCs overlaid each other, allowing for sub-population analysis and revealing 15 subpopulations of cells (**Figure 5B**). To determine the identity of these cells we did a differential gene expression analysis of each population against all other populations of cells to determine the top 10 genes expressed in each population. Based upon these gene signatures, we cross-referenced them to known gene makers of neural progenitor cell populations to classify

each population of cells **(Figure 5B)**. The clustered cell types expressed genes indicative of cells at different stages of differentiation and different progenitor populations. In general, similar proportions of control and Ts21 cells were in each subpopulation, although notable differences were observed **(Figure 5C)**. In particular, fewer CGE cells were present in Ts21 progenitors while the same proportion of MGE cells were present, corroborating our immunofluorescence (**Figure 2**). The larger proportion of ventral NPCs, and smaller proportion of both dorsal NPC and LGE cells and larger proportion of ventral NPCs in Ts21 suggest that Ts21 progenitors are patterned more ventrally. The increased proportion of midbrain NPCs together with decreased CGE suggest Ts21 are patterned less caudally. Interestingly, the results show an increased proportion of migrating interneurons, as defined by expression of DLX1, DLX2, DLX5 and DCX, in Ts21 that may indicate a premature transition from progenitor proliferation to migration in Ts21. Taken together, the scRNAseq results show that subpopulations in Ts21 ventralized progenitors differ from controls and suggest differences in patterning and differentiation.

We focused on differentially expressed genes between Ts21 and control in the MGE and CGE subpopulations to gain insight into pathways being altered in Ts21. We isolated the MGE and CGE populations in the Seurat analysis and performed differential gene expression analysis between the control and Ts21 cells in each population and used enrichR (Chen et al., 2013) to identify pathways dysregulated in each subpopulation (**Figure 5 D, E**). In the MGE subpopulation, most of the top pathways (involved in platelet function or reactive oxygen) were driven by expression of APP or SOD1, chromosome 21 encoded genes. GLI protein function also emerged as a dysregulated pathway in Ts21 MGE cells. In the CGE population, while some pathways emerged that were also driven by chromosome 21 gene expression (APP, SOD1, ATP50, CCT8), the major dysregulated pathway was WNT signaling that was driven by expression of non-chromosome 21 genes (SOX3, GNG2, RSPO3, RAC1, PFN1). These results corroborate our findings that Ts21 progenitors have defects in the balance of SHH and WNT signaling. Importantly, the results implicate signaling pathway differences specific to the CGE population and identify specific genes that drive these differences.

In addition to individual cell subpopulations, we want to know how gene expression relates to the trasitions among various subpoulations, especially in cell development. In particular, we want to get a deeper understanding of how the gene expression differences in the Ts21 CGE and MGE subpopulations affect their developmental trajectories,so we carried out pseudotime analysis of the scRNAseq data using Monocle (Trapnell et al., 2014). Monocle analysis revealed that all cell clusters (each of which corresponds to a particular subpopulation) in control and Ts21 progenitors generally have the same trajectories (**Figure 6A**), indicating that they are largely similar as we would expect based on the clustering data. However, the Ts21 trajectory has fewer transitions and the subpopulations are more distinct than controls, suggesting that the gene expression in Ts21 is potentially more subpopulation-specific than control. Moreover, the trajectories of MGE and CGE sub-population trajectories revealed additional differences between Ts21 and control. In the MGE subpopulation, the trajectories of control and Ts21 are similar but there are more cells in Ts21 in the later pseduotiming stage; i.e., the farthest right component (**Figure 6B**). We performed enrichment analysis on this population of cells (N=18) to define gene expression differences compared to all other cells in the subpopulation and identified specific pathways that were dysregulated. In the MGE population, 173 DEGs were identified and these genes were primarily in cell cycle, DNA repair and neural differentiation pathways. Interestingly, the genes identified in these Ts21 MGE outlier cells included ASCL1 and DLX transcription factors that are critical for interneuron development. Similar analysis of CGE cells identified far fewer DEGs (26 genes) in the population of CGE cells that was “missing” from controls and all of the genes were overexpressed compared to controls (**Figure 6C)**. These cells (N=11) have DEGs in neural differentiation, specifically interneuron differentiation and DNA binding pathways . Importantly, similar DEGs were identified in both MGE and CGE Ts21 outlier populations and included transcription factors ASCL1, DLX1, DLX2, DLX5, DCX and HES5. The expression of these particular genes suggests that Ts21 progenitors have more migratory cells in the MGE and CGE populations. This is corraborated by analysis of the migrating neuron cluster that shows expression of these genes and contains more Ts21 cells (**Figure 6D)**. These data suggest that Ts21 interneuron progenitors differentiate or migrate earlier than their control counterparts.

DISCUSSION

Results address gaps in both our understanding of human interneuron development and the consequences of mistakes in interneuron development. Interneuron development and function is a striking example of the failure of DS mouse models to recapitulate patient characteristics. DS mouse models show either more interneurons or no difference in interneuron populations (Chakrabarti et al., 2010; Goodliffe et al., 2016), *contrary to human brain data.* This discrepancy presents a serious problem in identifying therapeutic targets in DS. The predominant candidate mechanism underlying intellectual disability in DS that has emerged from research on mouse models is an imbalance in excitation-inhibition in the cortex, specifically over-inhibition and has led to the targeting of over-inhibition in the cortex by various drugs (Deidda et al., 2015; Gardiner, 2010; Martinez-Cue et al., 2014; Potier et al., 2014; Zorrilla de San Martin et al., 2018). These targets have not been validated in human patients and may lead to interventions that work in mouse but not in humans. Thus, human models are critical to identify therapeutic targets likely to impact and benefit human patients. (Zhao and Bhattacharyya, 2018).

Interneurons are more numerous, varied and elaborate in humans than in mouse. In mouse, 50% of interneurons are PV+, with CR+ constituting just 15-20%. Recent data suggests a greater contribution of interneuron subtypes from CGE progenitors in primates (Dzaja et al., 2014; Hansen et al., 2013; Hladnik et al., 2014; Ma et al., 2013) and our results corroborate this as we find a larger proportion of CR+ neurons in the STG compared to PV+. The data thus far link COUP-TFII+ progenitors and CR+ neurons, but differentiation of these progenitors has not been defined in human.

Our data appear to contradict a recently published paper that concluded that more interneurons are generated from Ts21 iPSCs (Xu et al., 2019). It is important to point out that some technical differences are likely responsible for the discrepancies in results and interpretation. Besides 3D versus 2D, we are using an unbiased approach to assess interneuron progenitors from Ts21 iPSCs, while they selected OLIG2+ cells for analysis. We are looking at an early timepoint (Day 17) when progenitors have established their positional identity while their analysis was at a later timepoint in organoids. Timing is critically important for generation of interneurons and so the results may be in agreement and we are just looking at different populations at different developmental times. However, in linking results with human brain data, they used Western blots to conclude that there are more calretinin neurons in DS, the first piece of data to show more neurons in *human* DS brain. We used a more rigorous approach of counting neurons with stereology to find fewer calretinin neurons and our data corroborates published human data.

WNT signaling is used in a tightly regulated and spatially specific manner during development of the forebrain to regulate regional forebrain identity, so the defects we have identified can be extended to other cortical neuronal populations to help us understand reduced neurogenesis in DS. The results focus on *spatial patterning* of interneuron progenitor populations. However, progenitors are also *temporally specified*. In fact, upper layer neurons and CGE develop later than other regions. Thus, it will be important to follow up these studies to define dynamic temporal patterning in DS.

METHODS

Quantification of neurons in post-mortem brain

Adult postmortem brain tissue was obtained from the NICHD Brain and Tissue Bank for Developmental Disorders with approval from the University of Wisconsin-Madison Institutional Review Board. The superior temporal gyrus or Brodmann's Area 22 was obtained from five DS individuals and five age and gender matched control subjects (**Table**). Tissues were sectioned at 50 microns using a cryostat and processed for immunocytochemistry.

Disorder	Age	Sex	Race
Control	15	Male	Caucasian
Ts21	15	Male	Caucasian
Control	19	Male	Caucasian
Ts21	19	Male	Caucasian
Control	19	Male	Caucasian
Ts21	19	Male	Caucasian
Control	23	Male	Caucasian
Ts21	23	Male	Caucasian
Control	24	Male	Afr Amer
Ts21	25	Male	Afr Amer
Control	32	Male	Caucasian
Ts21	33	Male	Caucasian

Immunocytochemistry: Antigen-antibodies were visualized with avidin-biotin, horseradish peroxidase (HRP) and 3, 3'-Diaminobenzidine (DAB) using standard immunohistochemical techniques. See **Table** for antibodies and staining conditions.

MARKER		ANTIBODY INFORMATION	ANTIGEN RETRIEVAL	DILUTION	secondary, ABC	DAB
all neurons	NeuN	AbCAM ab104225 Rabbit	Vector unmasking 15 minutes 95C	1:500	Visucyte HRP polymer	5 minutes ImPACT
Parvalbumin	PV	Sigma P3088 mouse	universal 5 min 95C or Vector	1:1000	Biotin 2' ABC	5 min
Calretinin	CR	7697 Rabbit	Vector unmasking 15 minutes 95C	1:2000	Biotin 2' ABC	3 minutes

Quantification of positive cells: The total numbers of PV+, CR+, and NeuN+ neurons were estimated using the Optical Fractionator (OF) workflow in Stereo Investigator software (MBF Bioscience). Six to eight sections at an interval of 5-7 were analyzed. Percentages of tissue for sampling were chosen based on the resample oversample function in Stereo Investigator (PV: 1%, CR: 1%, and NeuN: 0.5%) to ensure a coefficient of error < 0.1.The total positive cell count was estimated using the following equation: $N = \sum Q * \frac{t}{h} * \frac{1}{asf} * \frac{1}{ssf}$, where $\sum Q$is the total number of cells counted, *t* the average section thickness and *h* the height of the optical dissector, and *asf* and *ssf* the area sectioning fraction and the section sampling fractions, respectively [10].

Volume of tissue and density calculation: The total volume of tissue sampled and counted was estimated using the Cavalieri Estimator probe (Stereo Investigator, MBF Bioscience). The total cell population estimate (from the Optical Fractionator Workflow) was divided by the total tissue volume (from the Cavalieri Estimator) to calculate cell density.

Human induced pluripotent stem cells (iPSCs)

iPSCs were maintained on MEFs in hESC media (DMEM/F-12/KSOR/L-Glut/MEM-NEAA/FGF-20). Differentiation to interneuron progenitors was carried out as described (Liu et al., 2013).

Cell line	Sex	Age (years)	Karyotype	Relationship
WC-24-B	Female	25	Normal	Isogenic pair
WC-24-M			Trisomy 21	
DS2U	Male	1	Normal	Isogenic pair
DS1			Trisomy 21	
603-8	Male	36	Normal	Unrelated
WC-38-01	Male	35	Trisomy 21	
WC-58-07	Female	Neonate	Normal	Unrelated
WC-20-02	Female	3	Trisomy 21	

Cell proliferation: Cell proliferation was assayed using Click-iT™ EdU Alexa Fluor™ 488 Imaging Kit (Cat # C10337, ThermoFisher). Briefly, 10mM EdU stock solution was diluted to 20uM in NIM. Half of the media in the

well was removed and replaced with an equivalent volume of 20uM EdU for a final concentration of 10uM EdU. Cells were placed back in to the incubator for 8 hours. Cells were fixed with 4% paraformaldehyde in PBS for 15 minutes.

Gene	forward	reverse
AXIN2	5' TAT CCA GTG ATG CGC TGA CG-3'	5'-CGG TGG GTT CTC GGG AAA TG-3'
NR2F2/COUPTF2	5'-CTC AAG GCC ATA GTC CTG TCC-3'	5'-GGT ACT GGC TCC TAA CGT ATT C-3'
FZD1	5'- ATC TTC TTG TCC GGC TGT TAC A-3'	5'- GTC CTC GGC GAA CTT GTC ATT-3'
GLI- 1 h	5'-AAC GCT ATA CAG ATC CTA GCT CG-3'	5'- GTG CCG TTT GGT CAC ATG G-3'
GLI-2 h	5'-CCC CTA CCG ATT GAC ATG CG-3'	5'- GAA AGC CGG ATC AAG GAG ATG-3'
GLI-3 h	5'-GAA GTG CTC CAC TCG AAC AGA-3'	5'- GTG GCT GCA TAG TGA TTG CG-3'
LEF1	5'-ATG TCA ACT CCA AAC AAG GCA-3'	5'- CCC GGA GAC AAG GGA TAA AAA GT-3'
LRP5	5'-CGA CAC TGG GAC CAA CAG AA-3'	5'- AGA TGT AGC CCT TGG TGG GA-3'
LRP6	5'-CTG AGA GCG GCC CCT TTG TT-3'	5'-GCA TCC TCC AAG CCT CCA AC-3'
NKX2.1	5'-AGC ACA CGA CTC CGT TCT C-3'	5'-GCC CAC TTT CTT GTA GCT TTC C-3'
PTCH1	5'-GGA GCA GAT TTC CAA GGG GA-3'	5'-CCA CAA CCA AGA ACT TGC CG-3'
PTCH2	5'- CCG CCA GAG GTG ATA CAG AT-3'	5'-CCA CGG TCA TGG AGG TAG TC-3'
SMO	5'-ACT TGG ATT GCG AGG CTA GG-3'	5'- TCG CAA ACT TTG GAA CCC G-3'

Analysis

Immunofluorescence: On D17 or D25, neural progenitors plated on to laminin coated 96 well cell culture plates at 50-60,000 cells/well. The day after plating, cells were they then fixed with 4% paraformaldehyde in PBS for 15 minutes. Cells were rinsed with PBS and then incubated with a permeabilization/blocking buffer (5% normal goat serum, 0.1% TritonX-100 in PBS) for 30 minutes. Cells were incubated with primary antibodies overnight followed by fluorescent secondary antibodies, washed with PBS and mounted. Antibodies used were against NKX2.1 (abcam #EP1584Y, TTF) and COUP-TII (R&D Systems #PP-H7147-00).

High Content Imaging analysis: Imaging and analysis was done using the high content imager Operetta (Perkin Elmer) at 20x magnification.

RNA isolation and qPCR: RNA was isolated from progenitors using the ZYMO Research Direct-Zol RNA Miniprep plus (Cat #R2070) kit followed by cDNA synthesis using qScript cDNA supermix (Quanta bio). qPCR was done in triplicate on 2-3 batches of differentiation.

Microarray Gene Expression: RNA was isolated using the OMEGA (bio-tek) EZNA Total RNA I (Cat# R6834-01) kit. Isolated RNA was QC'd and hybridized to Applied Biosystems GeneChip™ Human Transcriptome Array 2.0 by the University of Wisconsin Biotechnology Center. Analysis was carried out using the Expression Console™ Software and TAC Software.

Single Cell RNA sequencing: Progenitor cells were analyzed using the 10x Genomics Chromium Single Cell Gene Expression Assay at the University of Wisconsin Biotechnology Center.

References

Alfano, C., Magrinelli, E., Harb, K., and Studer, M. (2014). The nuclear receptors COUP-TF: a long-lasting experience in forebrain assembly. Cellular and molecular life sciences : CMLS *71*, 43-62.

Anderson, S.A. (2002). Determination of cell fate within the telencephalon. Chemical senses *27*, 573-575.

Anderson, S.A., Kaznowski, C.E., Horn, C., Rubenstein, J.L., and McConnell, S.K. (2002). Distinct origins of neocortical projection neurons and interneurons in vivo. Cerebral cortex *12*, 702-709.

Becker, L.E. (1991). Synaptic dysgenesis. CanJNeurolSci *18*, 170-180.

Becker, L.E., Mito, T., Takashima, S., and Onodera, K. (1991). Growth and development of the brain in Down syndrome. Progress in clinical and biological research *373*, 133-152.

Benda, C.E. (1947). Mongolism and cretinism (New York: Grune and Stratton).

Bhattacharyya, A., McMillan, E., Chen, S.I., Wallace, K., and Svendsen, C.N. (2009). A critical period in cortical interneuron neurogenesis in Down syndrome revealed by human neural progenitor cells. Developmental neuroscience *31*, 497-510.

Boyce, R.W., Dorph-Petersen, K.A., Lyck, L., and Gundersen, H.J. (2010). Design-based stereology: introduction to basic concepts and practical approaches for estimation of cell number. ToxicolPathol *38*, 1011-1025.

Butler, A., Hoffman, P., Smibert, P., Papalexi, E., and Satija, R. (2018). Integrating single-cell transcriptomic data across different conditions, technologies, and species. Nature biotechnology *36*, 411-420.

Campbell, K. (2003). Dorsal-ventral patterning in the mammalian telencephalon. Current opinion in neurobiology *13*, 50-56.

Chakrabarti, L., Best, T.K., Cramer, N.P., Carney, R.S., Isaac, J.T., Galdzicki, Z., and Haydar, T.F. (2010). Olig1 and Olig2 triplication causes developmental brain defects in Down syndrome. NatNeurosci *13*, 927-934.

Chen, E.Y., Tan, C.M., Kou, Y., Duan, Q., Wang, Z., Meirelles, G.V., Clark, N.R., and Ma'ayan, A. (2013). Enrichr: interactive and collaborative HTML5 gene list enrichment analysis tool. BMC Bioinformatics *14*, 128.

Colon, E.J. (1972). The structure of the cerebral cortex in Down's Syndrome: a quantitative analysis. Neuropadiatrie *3*, 376.

Davidoff, L.M. (1928). The brain in mongolian idiocy: a report of ten cases. Arch Neurol Psychiay *20*, 1229.

Deidda, G., Parrini, M., Naskar, S., Bozarth, I.F., Contestabile, A., and Cancedda, L. (2015). Reversing excitatory GABAAR signaling restores synaptic plasticity and memory in a mouse model of Down syndrome. Nat Med *21*, 318-326.

Du, T., Xu, Q., Ocbina, P.J., and Anderson, S.A. (2008). NKX2.1 specifies cortical interneuron fate by activating Lhx6. Development *135*, 1559-1567.

Dzaja, D., Hladnik, A., Bicanic, I., Bakovic, M., and Petanjek, Z. (2014). Neocortical calretinin neurons in primates: increase in proportion and microcircuitry structure. Frontiers in neuroanatomy *8*, 103.

Emerson, J.F., Kesslak, J.P., Chen, P.C., and Lott, I.T. (1995). Magnetic resonance imaging of the aging brain in Down syndrome. ProgClinBiolRes *393*, 123-138.

Gardiner, K.J. (2010). Molecular basis of pharmacotherapies for cognition in Down syndrome. Trends PharmacolSci *31*, 66-73.

Golden, J.A., and Hyman, B.T. (1994). Development of the superior temporal neocortex is anomalous in trisomy 21. JNeuropatholExpNeurol *53*, 513-520.

Goodliffe, J.W., Olmos-Serrano, J.L., Aziz, N.M., Pennings, J.L., Guedj, F., Bianchi, D.W., and Haydar, T.F. (2016). Absence of Prenatal Forebrain Defects in the Dp(16)1Yey/+ Mouse Model of Down Syndrome. The Journal of neuroscience : the official journal of the Society for Neuroscience *36*, 2926-2944.

Gulacsi, A., and Anderson, S.A. (2006). Shh maintains Nkx2.1 in the MGE by a Gli3-independent mechanism. Cerebral cortex *16 Suppl 1*, i89-95.

Hansen, D.V., Lui, J.H., Flandin, P., Yoshikawa, K., Rubenstein, J.L., Alvarez-Buylla, A., and Kriegstein, A.R. (2013). Non-epithelial stem cells and cortical interneuron production in the human ganglionic eminences. Nature neuroscience *16*, 1576-1587.

Hladnik, A., Dzaja, D., Darmopil, S., Jovanov-Milosevic, N., and Petanjek, Z. (2014). Spatio-temporal extension in site of origin for cortical calretinin neurons in primates. Frontiers in neuroanatomy *8*, 50.

Huo, H.Q., Qu, Z.Y., Yuan, F., Ma, L., Yao, L., Xu, M., Hu, Y., Ji, J., Bhattacharyya, A., Zhang, S.C.*, et al.* (2018). Modeling Down Syndrome with Patient iPSCs Reveals Cellular and Migration Deficits of GABAergic Neurons. Stem cell reports *10*, 1251-1266.

Kanatani, S., Yozu, M., Tabata, H., and Nakajima, K. (2008). COUP-TFII is preferentially expressed in the caudal ganglionic eminence and is involved in the caudal migratory stream. The Journal of neuroscience : the official journal of the Society for Neuroscience *28*, 13582-13591.

Kesslak, J.P., Nagata, S.F., Lott, I., and Nalcioglu, O. (1994). Magnetic resonance imaging analysis of age-related changes in the brains of individuals with Down's syndrome. Neurology *44*, 1039-1045.

Li, X.J., Zhang, X., Johnson, M.A., Wang, Z.B., Lavaute, T., and Zhang, S.C. (2009). Coordination of sonic hedgehog and Wnt signaling determines ventral and dorsal telencephalic neuron types from human embryonic stem cells. Development *136*, 4055-4063.

Liu, Y., Liu, H., Sauvey, C., Yao, L., Zarnowska, E.D., and Zhang, S.C. (2013). Directed differentiation of forebrain GABA interneurons from human pluripotent stem cells. Nature protocols *8*, 1670-1679.

Lodato, S., Tomassy, G.S., De Leonibus, E., Uzcategui, Y.G., Andolfi, G., Armentano, M., Touzot, A., Gaztelu, J.M., Arlotta, P., Menendez de la Prida, L.*, et al.* (2011). Loss of COUP-TFI alters the balance between caudal ganglionic eminence- and medial ganglionic eminence-derived cortical interneurons and results in resistance to epilepsy. The Journal of neuroscience : the official journal of the Society for Neuroscience *31*, 4650-4662.

Lott, I.T., and Dierssen, M. (2010). Cognitive deficits and associated neurological complications in individuals with Down's syndrome. Lancet Neurol *9*, 623-633.

Ma, T., Wang, C., Wang, L., Zhou, X., Tian, M., Zhang, Q., Zhang, Y., Li, J., Liu, Z., Cai, Y.*, et al.* (2013). Subcortical origins of human and monkey neocortical interneurons. Nature neuroscience *16*, 1588-1597.

Martinez-Cue, C., Delatour, B., and Potier, M.C. (2014). Treating enhanced GABAergic inhibition in Down syndrome: use of GABA alpha5-selective inverse agonists. Neuroscience and biobehavioral reviews *46 Pt 2*, 218-227.

Mito, T., Pereyra, P.M., and Becker, L.E. (1991). Neuropathology in patients with congenital heart disease and Down syndrome. PediatrPathol *11*, 867-877.

Olmos-Serrano, J.L., Kang, H.J., Tyler, W.A., Silbereis, J.C., Cheng, F., Zhu, Y., Pletikos, M., Jankovic-Rapan, L., Cramer, N.P., Galdzicki, Z.*, et al.* (2016). Down Syndrome Developmental Brain Transcriptome Reveals Defective Oligodendrocyte Differentiation and Myelination. Neuron *89*, 1208-1222.

Parnavelas, J.G., Anderson, S.A., Lavdas, A.A., Grigoriou, M., Pachnis, V., and Rubenstein, J.L. (2000). The contribution of the ganglionic eminence to the neuronal cell types of the cerebral cortex. Novartis Foundation symposium *228*, 129-139; discussion 139-147.

Perl, D.P., Good, P.F., Bussiere, T., Morrison, J.H., Erwin, J.M., and Hof, P.R. (2000). Practical approaches to stereology in the setting of aging- and disease-related brain banks. Journal of chemical neuroanatomy *20*, 7-19.

Potier, M.C., Braudeau, J., Dauphinot, L., and Delatour, B. (2014). Reducing GABAergic inhibition restores cognitive functions in a mouse model of Down syndrome. CNS & neurological disorders drug targets *13*, 8-15.

Reinchisi, G., Ijichi, K., Glidden, N., Jakovcevski, I., and Zecevic, N. (2012). COUP-TFII expressing interneurons in human fetal forebrain. Cerebral cortex *22*, 2820-2830.

Ross, M.H., Galaburda, A.M., and Kemper, T.L. (1984). Down's syndrome: is there a decreased population of neurons? Neurology *34*, 909-916.

Schmidt-Sidor, B., Wisniewski, K.E., Shepard, T.H., and Sersen, E.A. (1990). Brain growth in Down syndrome subjects 15 to 22 weeks of gestational age and birth to 60 months. ClinNeuropathol *9*, 181-190.

Takashima, S., Becker, L.E., Armstrong, D.L., and Chan, F. (1981). Abnormal neuronal development in the visual cortex of the human fetus and infant with down's syndrome. A quantitative and qualitative Golgi study. Brain Res *225*, 1-21.

Trapnell, C., Cacchiarelli, D., Grimsby, J., Pokharel, P., Li, S., Morse, M., Lennon, N.J., Livak, K.J., Mikkelsen, T.S., and Rinn, J.L. (2014). The dynamics and regulators of cell fate decisions are revealed by pseudotemporal ordering of single cells. Nature biotechnology *32*, 381-386.

Weitzdoerfer, R., Dierssen, M., Fountoulakis, M., and Lubec, G. (2001). Fetal life in Down syndrome starts with normal neuronal density but impaired dendritic spines and synaptosomal structure. JNeural TransmSuppl, 59-70.

West, M.J. (2013). Optimizing the sampling scheme for a stereological study: how many individuals, sections, and probes should be used. Cold Spring HarbProtoc *2013*.

West, M.J., Slomianka, L., and Gundersen, H.J. (1991). Unbiased stereological estimation of the total number of neurons in thesubdivisions of the rat hippocampus using the optical fractionator. AnatRec *231*, 482-497.

Wilson, S.W., and Rubenstein, J.L. (2000). Induction and dorsoventral patterning of the telencephalon. Neuron *28*, 641-651.

Wisniewski, K.E. (1990). Down syndrome children often have brain with maturation delay, retardation of growth, and cortical dysgenesis. AmJMedGenetSuppl *7*, 274-281.

Wisniewski, K.E., Laure-Kamionowska, M., and Wisniewski, H.M. (1984). Evidence of arrest of neurogenesis and synaptogenesis in brains of patients with Down's syndrome. NEnglJMed *311*, 1187-1188.

Xu, Q., Guo, L., Moore, H., Waclaw, R.R., Campbell, K., and Anderson, S.A. (2010). Sonic hedgehog signaling confers ventral telencephalic progenitors with distinct cortical interneuron fates. Neuron *65*, 328-340.

Xu, Q., Tam, M., and Anderson, S.A. (2008). Fate mapping Nkx2.1-lineage cells in the mouse telencephalon. The Journal of comparative neurology *506*, 16-29.

Xu, Q., Wonders, C.P., and Anderson, S.A. (2005). Sonic hedgehog maintains the identity of cortical interneuron progenitors in the ventral telencephalon. Development *132*, 4987-4998.

Xu, R., Brawner, A.T., Li, S., Liu, J.J., Kim, H., Xue, H., Pang, Z.P., Kim, W.Y., Hart, R.P., Liu, Y.*, et al.* (2019). OLIG2 Drives Abnormal Neurodevelopmental Phenotypes in Human iPSC-Based Organoid and Chimeric Mouse Models of Down Syndrome. Cell stem cell *24*, 908-926 e908.

Zhang, F., Wu, Y., and Tian, W. (2019). A novel approach to remove the batch effect of single-cell data. Cell Discovery *5*, 46.

Zhao, X., and Bhattacharyya, A. (2018). Human Models Are Needed for Studying Human Neurodevelopmental Disorders. American journal of human genetics *103*, 829-857.

Zorrilla de San Martin, J., Delabar, J.M., Bacci, A., and Potier, M.C. (2018). GABAergic over-inhibition, a promising hypothesis for cognitive deficits in Down syndrome. Free radical biology & medicine *114*, 33-39.

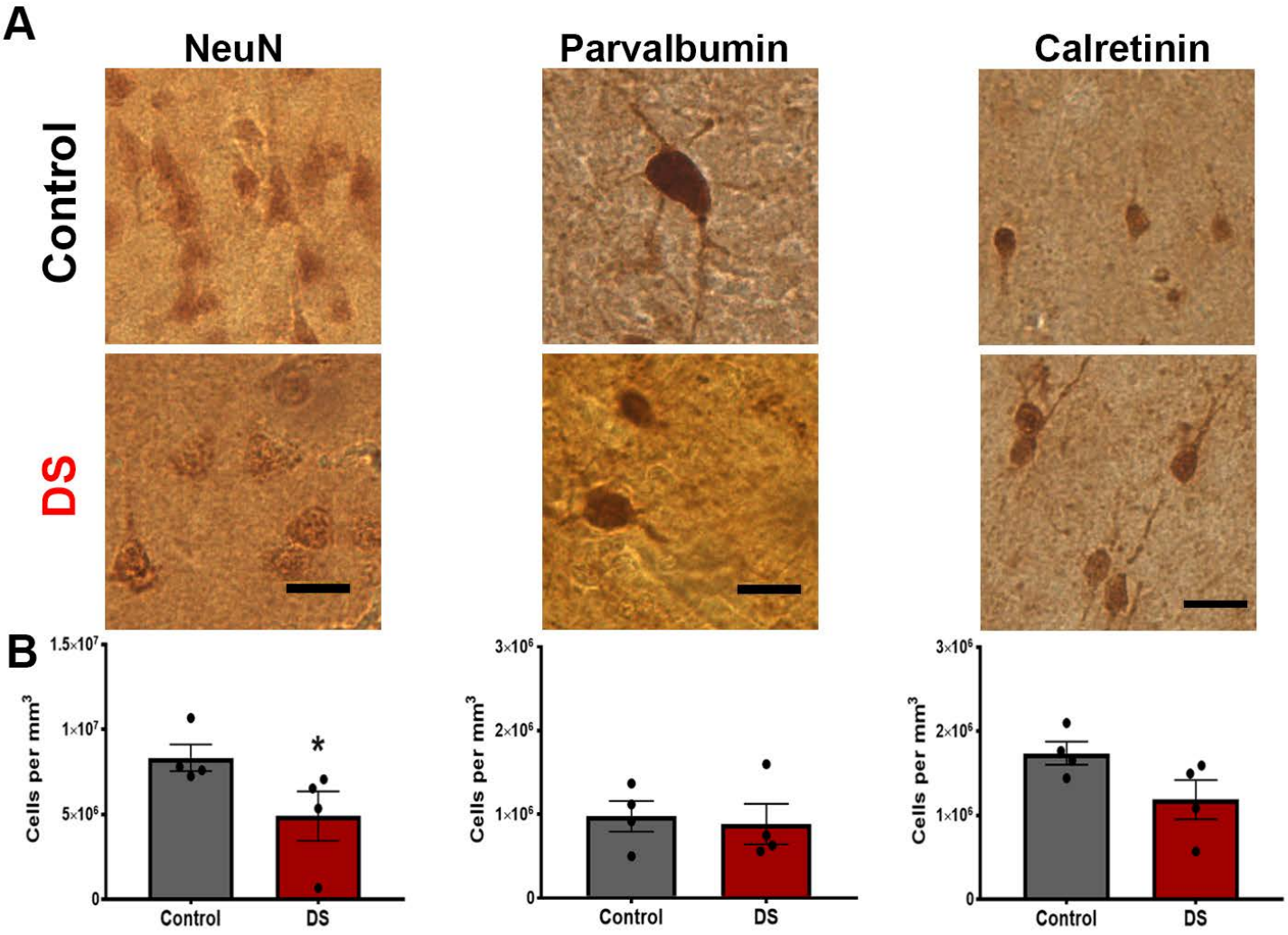

Figure 1: Reduced density of neurons in post-mortem Down syndrome cortex.
A) Representative images of NeuN+, PV+ and CR+ neurons detected by immunohistochemistry (DAB) in control and DS post-mortem superior temporal gyrus (STG) samples. **B)** Stereological quantification of the density of NeuN+ neurons, parvalbumin (PV) positive and calretinin (CR) positive neurons in control and DS tissue. (p-value calculated using non-parametric Mann-Whitney test, N=4).

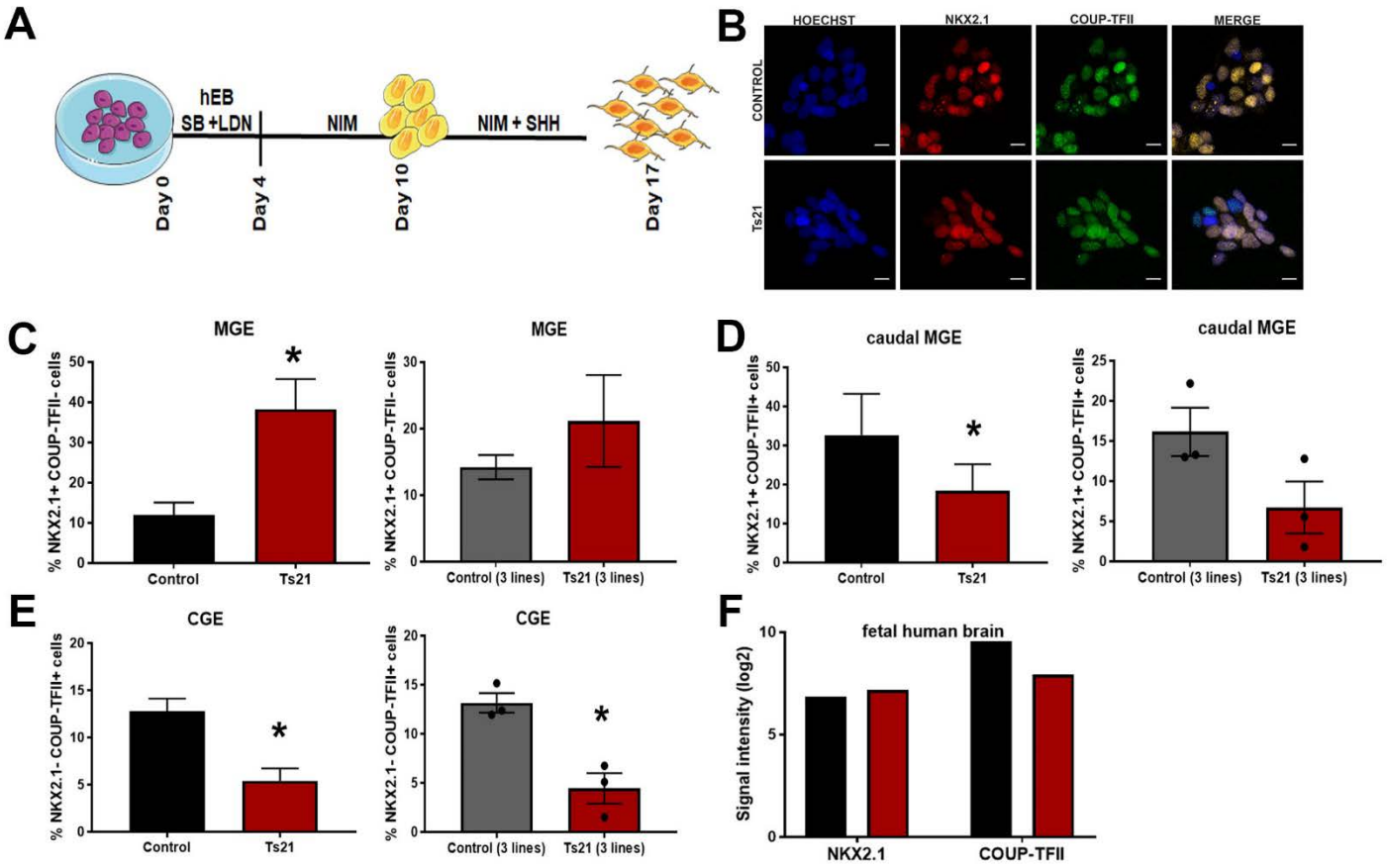

Figure 2: Ventralization results in altered patterning of isogenic Ts21 iPSCs
A) Schematic of interneuron progenitor differentiation protocol with cells harvested at Day 17. **B)** Representative immunofluorescence images of NKX2.1+ and COUP-TFII+ nuclei in control and Ts21 isogenic neural progenitor cells at Day 17 of differentiation. **C)** Quantification of NKX2.1+ COUP-TFII+ nuclei in control and Ts21 isogenic neural progenitor cells at Day 17 shows that Ts21 cells have more NKX2.1+ COUP-TFII- (MGE) cells than controls. Similar reduction is observed in 3 other DS and control lines. **D)** Quantification of NKX2.1+ COUP-TFII+ nuclei in control and Ts21 isogenic neural progenitor cells at Day 17 shows that Ts21 cells have fewer NKX2.1+ COUP-TFII+ (caudal MGE) cells than controls. Similar reduction is observed in 3 other DS and control lines. **E)** Quantification of NKX2.1+ COUP-TFII+ nuclei in control and Ts21 isogenic neural progenitor cells at Day 17 shows that Ts21 cells have fewer NKX2.1- COUP-TFII+ (CGE) cells than controls. Similar reduction is observed in 3 other DS and control lines. **F)** Expression of NKX2.1 and COUP-TFII in human fetal control and Down syndrome brain (14-17 weeks gestation, dorsolateral forebrain) (Olmos-Serrano et al., 2016) shows less COUP-TFII+ expression in Down syndrome.

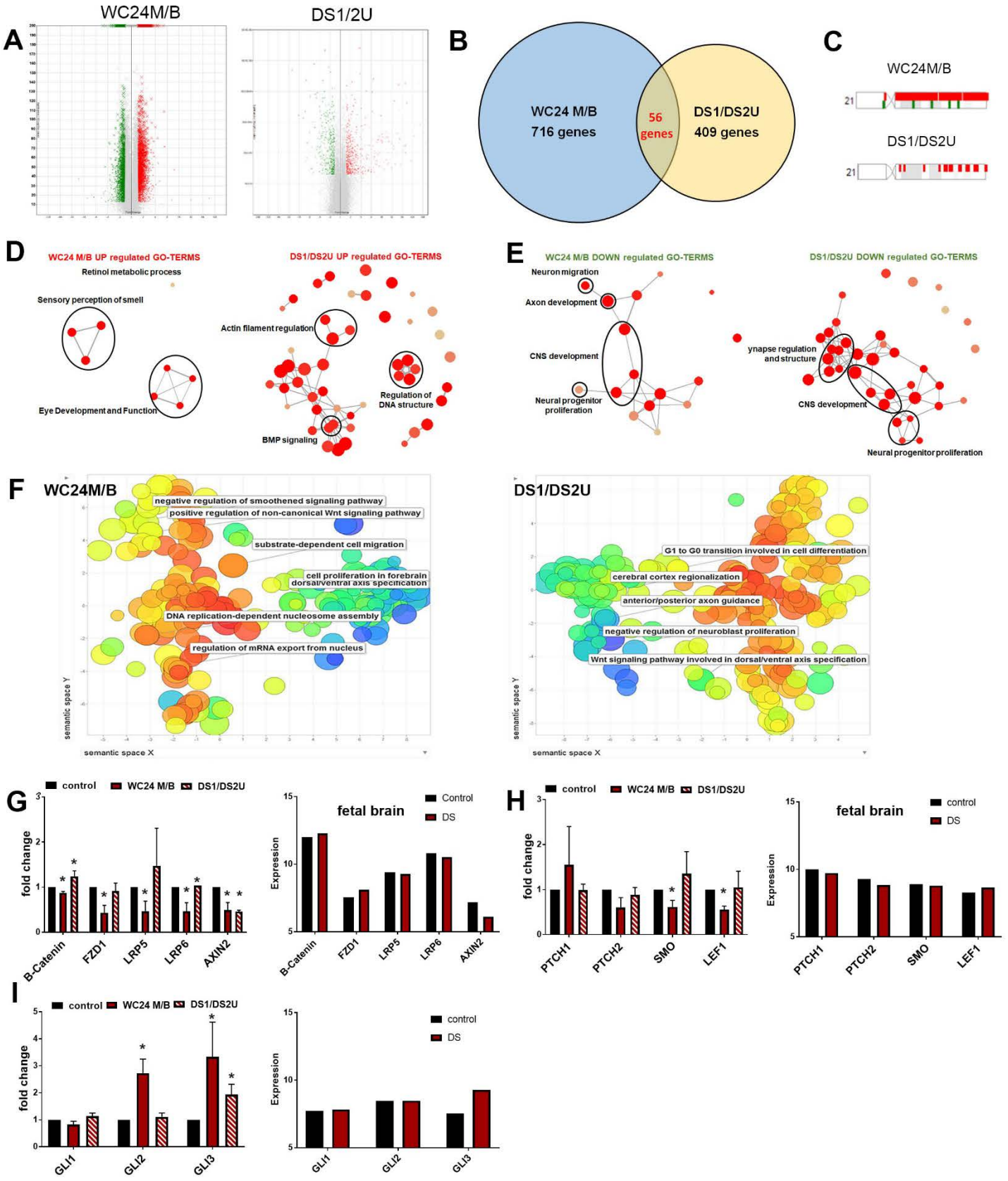

Figure 3: Microarray analysis of two isogenic pairs of Ts21 and control ventralized progenitors reveals defects in WNT signaling.

A) Volcano plots show overall gene expression changes in ventralized progenitors (Day 25) from two isogenic pairs of Ts21 and control iPSCs (WC24M/B and DS1/DS2U). **B)** The two sets of cells have distinct and overlapping differentially expressed genes. **C)** Gene expression changes on HSA21 for each set. **D)** Enrichment of Gene Ontology (GO) processes up-regulated in differential expressed genes in each set of isogenic cells. **E)** Enrichment of G) processes down-regulated in differential expressed genes in each set of isogenic cells. **F)** Gene clusters identified in differential expressed genes in each set of isogenic cells. Red is increased and green is decreased expression in panels A, C. Quantitative pCR was used to validate the microarray results. Gene expression differences were not consistently observed in SHH pathway genes or in fetal brain (Olmos-Serrano et al., 2016) **(G)**, but were observed in WNT signaling genes **(H)** and GLI3 **(I)**.

TABLE 1: pathways identified in Ts21 versus control interneuron progenitors.

PATHWAYS	P-VALUE
Ectoderm Differentiation_Homo sapiens_WP2858	1.66E-05
Endoderm Differentiation_Homo sapiens_WP2853	0.000238
Neural Crest Differentiation_Homo sapiens_WP2064	0.000615
Preimplantation Embryo_Homo sapiens_WP3527	0.009457
Wnt Signaling Pathway and Pluripotency_Homo sapiens_WP399	0.011516
Mesodermal Commitment Pathway_Homo sapiens_WP2857	0.02565
Wnt Signaling Pathway_Homo sapiens_WP428	0.054853
Cadherin signaling pathway_Homo sapiens_P00012	2.97E-14
Wnt signaling pathway_Homo sapiens_P00057	1.34E-10
Alzheimer disease-presenilin pathway_Homo sapiens_P00004	0.000346
Angiogenesis_Homo sapiens_P00005	0.001248
Axon guidance mediated by Slit/Robo_Homo sapiens_P00008	0.000563
Ionotropic glutamate receptor pathway_Homo sapiens_P00037	0.017174
Notch signaling pathway_Homo sapiens_P00045	0.05116
Signaling pathways regulating pluripotency of stem cells_Homo sapiens_hsa04550	1.05E-07
Axon guidance_Homo sapiens_hsa04360	0.000526
Hippo signaling pathway_Homo sapiens_hsa04390	0.000609
Cell adhesion molecules (CAMs)_Homo sapiens_hsa04514	0.001248
Tight junction_Homo sapiens_hsa04530	0.003795
Wnt signaling pathway_Homo sapiens_hsa04310	0.004367
Hedgehog signaling pathway_Homo sapiens_hsa04340	0.004823

WIKIPATHWAYS
PANTHER
KEGG

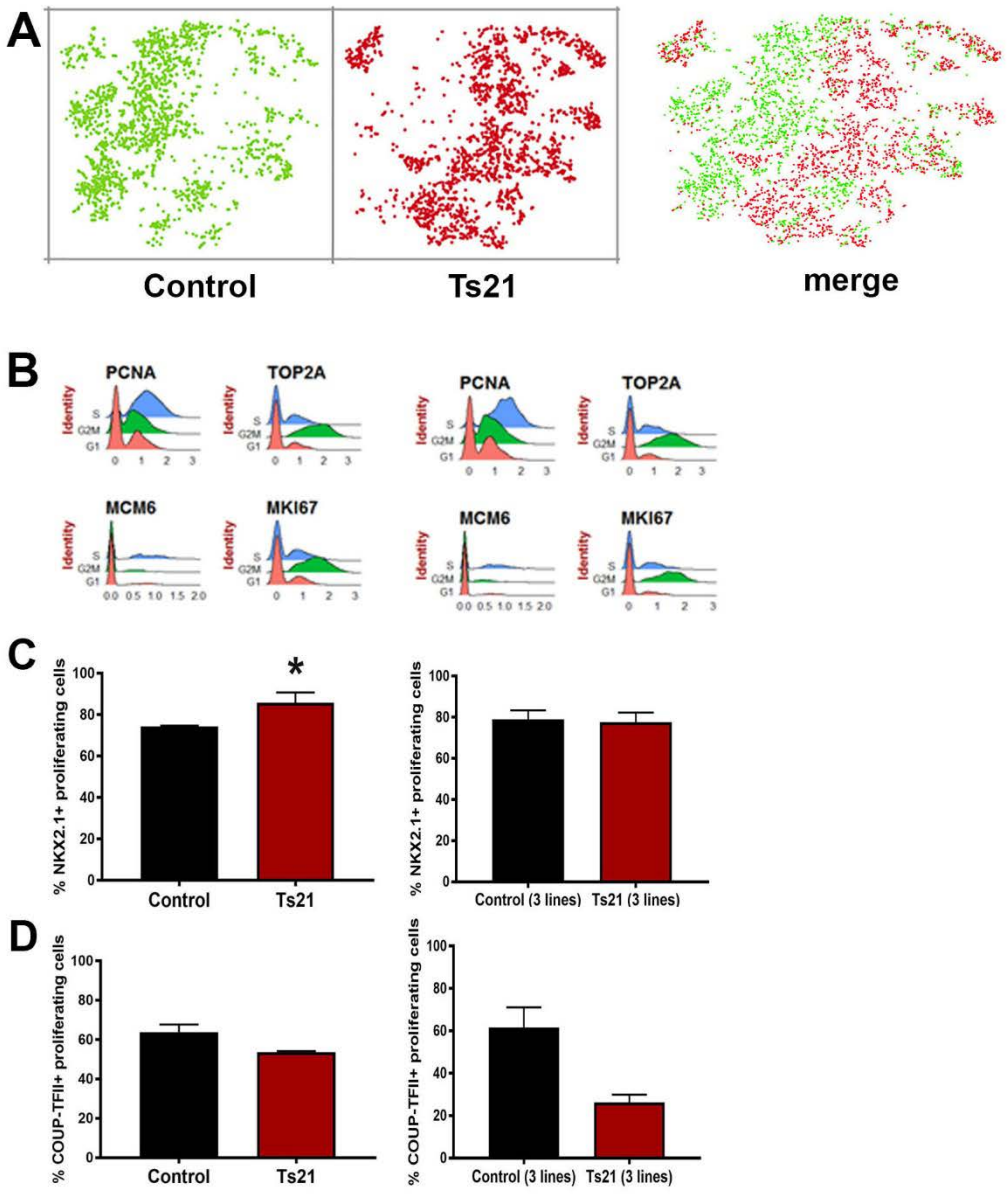

Figure 4: Proliferation differences in interneuron subpopulations. A) t-SNE plot of principal component analysis (PCA) comparing Ts21 to control scRNA-Seq data. **B)** Expression of PCNA, TOP2A, MCM6 and MKI67, is similar in Ts21 and control progenitors. **C)** NKX2.1+/EdU+ indicates proliferating cells in the Ts21 cells compared to their isogenic controls and in an additional three Ts21 and control iPSC lines. **D)** COUP-TII+/EdU+ indicates proliferating cells in the Ts21 cells compared to their isogenic controls and in an additional three Ts21 and control iPSC lines.

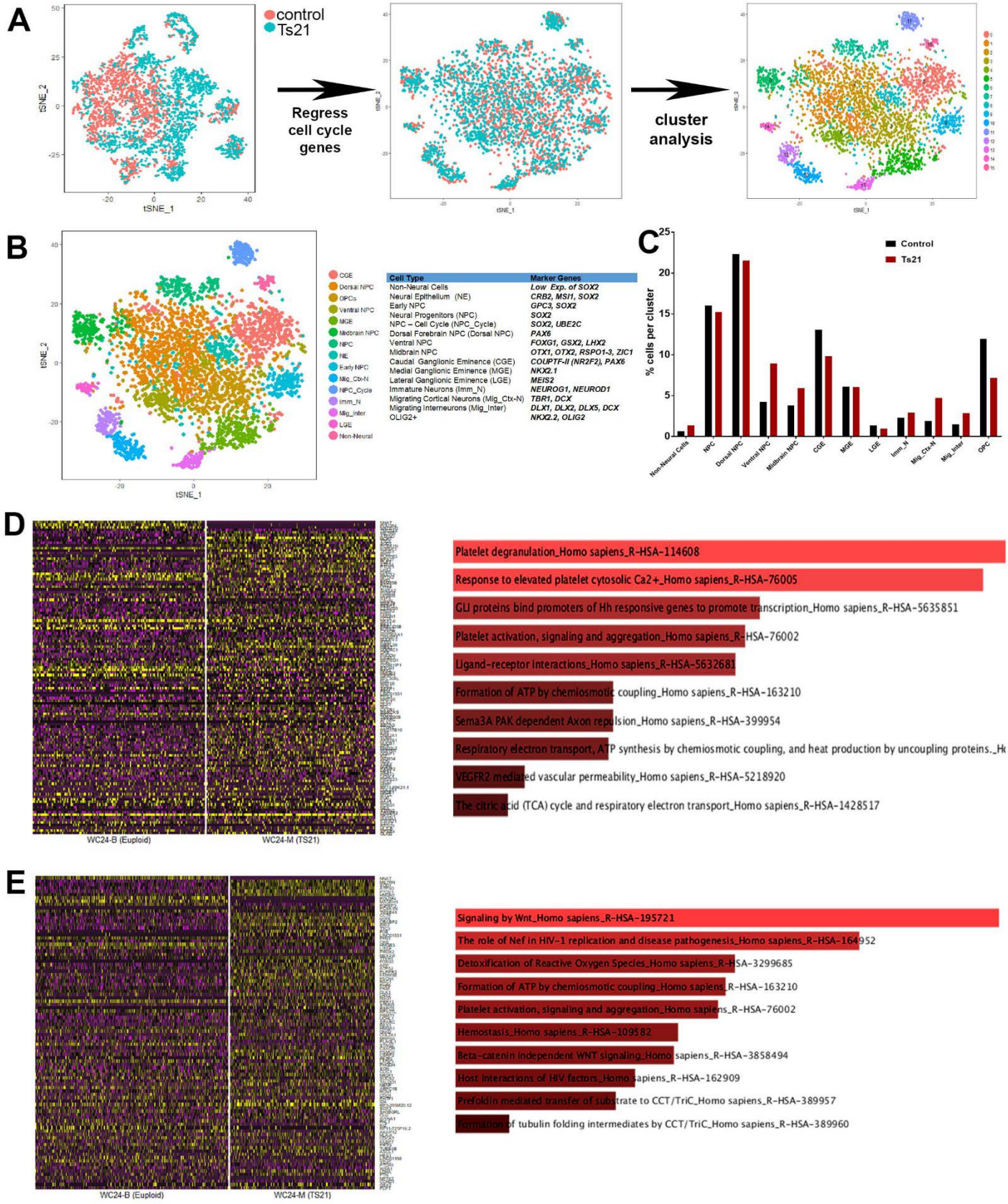

Figure 5: Single cell RNA-Seq reveals differences in Ts21 progenitor subpopulations

A) Schematic of work flow. t-SNE plot if initial PCA analysis shows almost complete segregation of the control and Ts21 neural progenitor cells (WC24 M/B). Seurat was used to regress out all the cell cycle genes. Clustering analysis revealed 15 sub-populations of cells. **B)** Sub-populations identities were based on expression of known

gene markers. **C)** Percentages of control and Ts21 cells in each cluster for control (2134 cells) and Ts21 (2158 cells). **D)** Differentially expressed genes in the NKX2.1+ (MGE) cluster and pathway analysis of these genes. **E)** Differentially expressed genes in the COUP-TFII+ (CGE) cluster and pathway analysis of these genes.

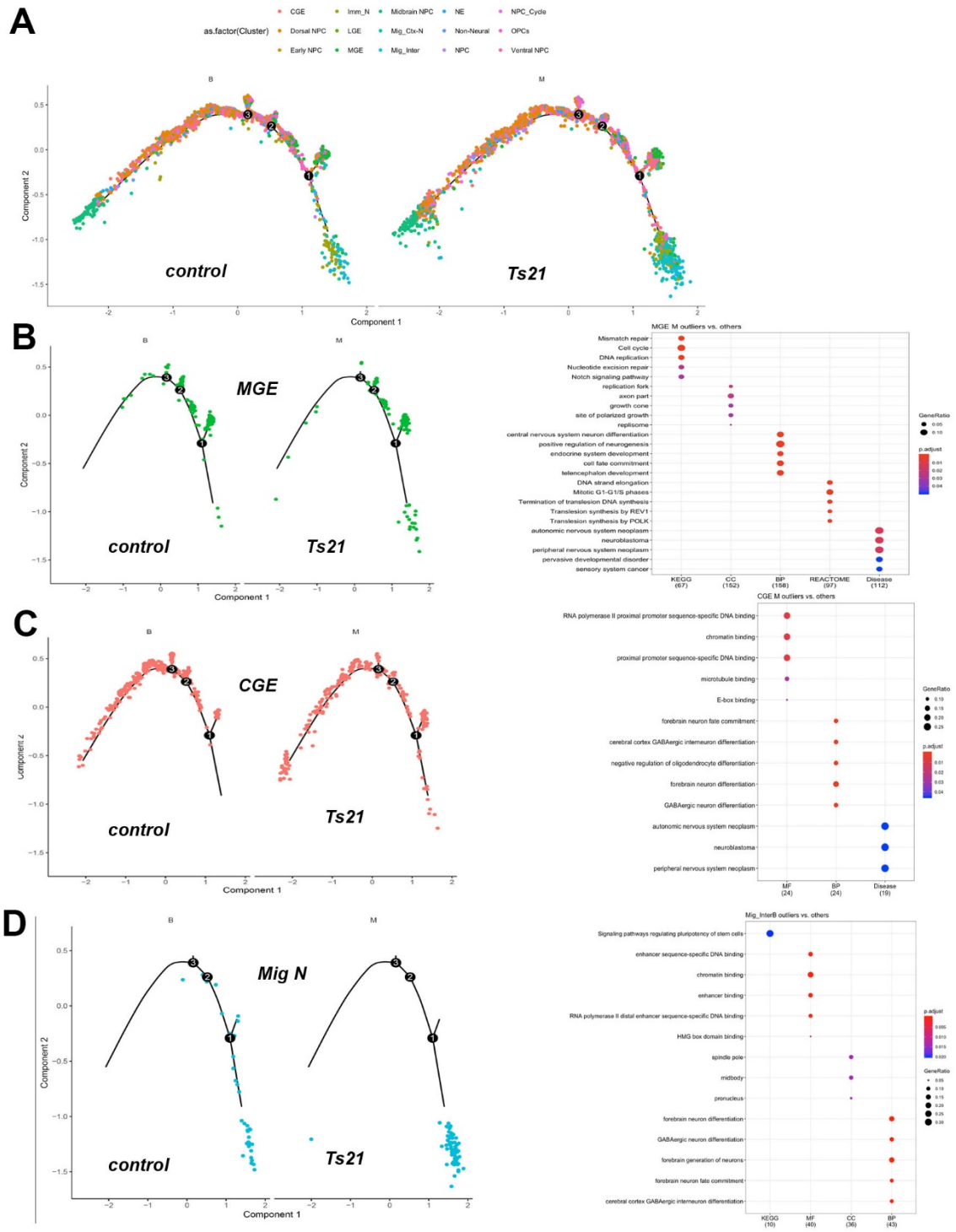

Figure 6: Pseudotiming of Ts21 versus control interneuron progenitors. A) Monocle analysis of all cell clusters (each of which corresponds to a particular subpopulation) in control and Ts21 progenitors. Trajectories of MGE **(B)** and CGE **(C)** and migrating neuron **(D)** sub-populations between Ts21 and control.